PHYSICAL REVIEW E, VOLUME 63, 065401(R)

Dynamics of Raman instabilities using chirped laser pulses

J. Faure,[1] J.-R. Marquès,[1] V. Malka,[1] F. Amiranoff,[1] Z. Najmudin,[2] B. Walton,[2] J.-P. Rousseau,[3] S. Ranc,[3] A. Solodov,[4] and P. Mora[4]

[1]*Laboratoire pour l'Utilisation des Lasers Intenses, UMR 7605, CNRS-CEA-Ecole Polytechnique-Université Pierre et Marie Curie, 91128 Palaiseau Cedex, France*

[2]*Blackett Laboratory, Imperial College, London, United Kingdom*

[3]*Laboratoire d'Optique Appliquée, Ecole Nationale Supérieure des Techniques avancées, 91128 Palaiseau, France*

[4]*Centre de Physique Théorique, UMR 7644 CNRS-Ecole Polytechnique, 91128 Palaiseau, France*

(Received 12 September 2000; published 24 May 2001)

Time resolved measurements of the growth of Raman instabilities were performed using a picosecond chirped laser pulse. It was observed experimentally that for a short laser pulse (<10 ps), forward and 30° Raman scattering occur at the back of the pulse. The growth of the instabilities was found to be independent of the sign of the chirp. In addition, a simple temporal model was developed and shows good agreement with the experimental results. This model also indicates that the plasma wave driven by forward Raman scattering is severely damped in the case of pulses longer than a few picoseconds. Damping by the modulational instability is compatible with the experimental results.

DOI: 10.1103/PhysRevE.63.065401 PACS number(s): 52.35.Mw, 52.38.−r, 52.75.Di

Raman instabilities [1] occur during the interaction of intense light with an underdense plasma for electron densities $n_e \leqslant n_c/4$, where n_c is the plasma critical density. Raman instabilities are usually described as a three wave process in which an incident electromagnetic (EM) wave $(\omega_0, \mathbf{k_0})$ decays resonantly into a scattered electromagnetic wave $(\omega_s, \mathbf{k_s})$ and a plasma wave $(\omega_{pe}, \mathbf{k_p})$, where ω_{pe} is the frequency of the electron plasma wave. These waves satisfy the dispersion relations in a plasma, as well as the phase matching conditions: $\omega_0 = \omega_s + \omega_{pe}$ and $\mathbf{k_0} = \mathbf{k_s} + \mathbf{k_p}$. These instabilities have been studied intensively for the past few decades because of their important role in inertial confinement fusion physics. In the interaction of a short (<10 ps) high intensity ($I \simeq 10^{18}$ W/cm^2) laser pulse with an underdense plasma, Raman instabilities also play an important role. For instance, in the laser-plasma accelerator concept [2,3], Raman forward scattering (RFS) can be used to drive relativistic plasma waves [4,5] which accelerate electrons to multi-MeV energies. This effect is also relevant for the fast ignitor [6] fusion scheme: the ultraintense laser pulse propagating in underdense regions of the expanding fusion target can produce hot electrons through Raman instabilities. Therefore, the study of the dynamics of the different Raman instabilities and their interplay is crucial to a better understanding of the interaction in these regimes.

For three wave Raman processes, the growth rate is [7]: $\gamma = kca_0/4[\omega_p^2/\omega_{pe}(\omega_0 - \omega_{pe})]^{1/2}$, where k is the plasma wave vector, ω_p the plasma frequency, a_0 the normalized potential vector, and ω_0 the laser central frequency. The plasma wave (or Bohm-Gross) frequency reads $\omega_{pe} = (\omega_p^2 + 3k^2 v_{th}^2)^{1/2}$, where v_{th} is the electron thermal velocity. The three wave Raman growth rate increases with the scattering angle and is maximum for Raman backward scattering (RBS). Hence one expects RBS to occur first, followed by Raman side scattering (RSS) and RFS. This has been observed in recent particle in cell (PIC) simulations: Tzeng *et al.* [8,9] simulated the interaction of an ultraintense laser pulse and showed that wavebreaking due to RBS and large angle RSS occurs at the beginning of the pulse, while RFS grows later in the pulse. This leads to a possible scenario for trapping [10,8]: RBS and RSS could preaccelerate electrons, enhancing the trapping in the fast plasma wave driven by RFS. This illustrates the important role of the instability dynamics on the understanding of trapping mechanisms.

The temporal evolution of the RFS-driven plasma wave has been measured before [11] using Thomson scattering. However, in this Rapid Communication, we assess the time in the referential of the laser pulse at which Raman instabilities occur. In this sense, our measurements give additional information on the dynamics of the instabilities. The temporal resolution was obtained by using a chirped pulse as the pump pulse. Although chirped pulses have been used before [12], here they have been used to investigate on the temporal dynamics of instabilities and they constitute a powerful tool for such a purpose.

The experiment was performed at the Laboratoire d'Optique Appliquée on the 10 Hz, 20 terawatt laser at $\lambda_0 = 820$ nm. The laser delivered up to 600 mJ in $\tau_0 = 35$ fs at full width half maximum (FWHM) and was focused with a $f/7.5$ off axis parabola to a focal spot of $w_0 = 6$ μm, where w_0 is the radius at $1/e$ in field amplitude. However, by translating one of the gratings of the compressor, we were able to generate chirped pulses with durations at FWHM ranging from $\tau_c = 35$ fs to 7 ps (and respective intensities from $I = 1.5 \times 10^{19}$ to $I = 8 \times 10^{16}$ W/cm^2). The chirped laser pulse was focused onto the edge of a supersonic helium gas jet. The neutral density profile of the jet was measured before the experiment [13]: it was flat over a plateau of 4 mm and the density gradient length at the edges was about 400 μm. In order to study the temporal dynamics of Raman instabilities, the transmitted light, the 30° side scattered light and the back-scattered light from the interaction were imaged onto the slit of a spectrometer. The spectra were recorded with a 16 bit charge-coupled-device camera.

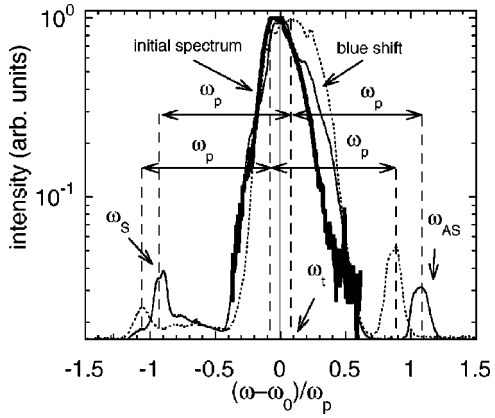

FIG. 1. Experimental RFS spectra for $\tau_c=4.2$ ps, $I=1.2\times10^{17}$ W/cm^2, $n_e=3\times10^{19}$ cm^{-3}. Solid (dotted) line: positive (negative) chirp. Thick solid line: initial spectrum.

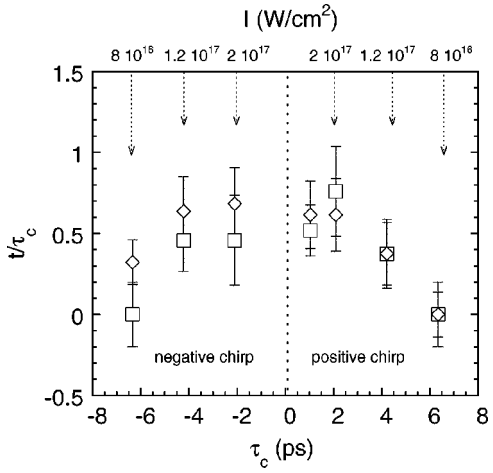

FIG. 2. Time of maximum scattering for RFS (open squares) and RSS (open diamonds) for different pulse durations and for $n_e=3\times10^{19}$ cm^{-3}. On the y axis, $t/\tau_c=0$ corresponds to the maximum intensity of the pulse.

For a chirped Gaussian pulse, one can define an instantaneous frequency: $\omega_t=\omega_0+2bt$, where b is the chirp parameter $b=2\ln2/\tau_c^2\sqrt{(\tau_c/\tau_0)^2-1}$, t the time in the pulse reference frame, and τ_c (τ_0) the duration at FWHM of the chirped (transform limited) pulse. Hence, for a positive (negative) chirp, $b>(<)0$ and the ''red'' (''blue'') frequencies are located at the front of the pulse.

If a plasma wave grows during the interaction an EM wave at frequency $\omega_s=\omega_{t_0}-\omega_{pe}$ is scattered. Its amplitude will reach a maximum at time t_0, and t_0 maximizes the product $E(t)\delta n(t)$, where δn is the amplitude of the density perturbation associated with the plasma wave and $E(t)$ the laser electric field. Hence, by measuring the spectrum of the scattered wave, one can retrieve the instantaneous frequency ω_{t_0}, and, as a consequence, obtain time resolution in the referential frame of the pulse.

The thin solid line of Fig. 1 shows a typical RFS experimental spectrum (transmitted light), obtained for a positive chirp. One can see the spectrum of the laser and two satellites: Stokes at $\omega_S=\omega_{t_0}-\omega_{pe}$ and anti-Stokes at $\omega_{AS}=\omega_{t_0}+\omega_{pe}$. These two satellites signify the presence of a plasma wave driven by RFS. Then, the instantaneous frequency is simply given by $\omega_{t_0}=(\omega_S+\omega_{AS})/2$, and one can retrieve the time of maximum scattering t_0 knowing the central frequency ω_0. The initial laser spectrum (thick solid line) was fitted by a Gaussian function, giving a central wavelength at $\lambda_0=813$ nm, which was used for the analysis . The dashed line in Fig. 1 shows the RFS spectrum obtained with the same parameters but for a negative chirp. In this case, the satellites are shifted because the frequency ω_{t_0} is different for a positive or a negative chirp. In Fig. 1, one can also notice that the central wavelength was somewhat blue shifted: this is the effect of ionization [14]. Ionization causes a frequency shift but it takes place early enough in the pulse so that RFS does not experience it.

This purely temporal analysis of the data neglects propagation effects. This assumption is justified because for all the data shown in this paper, the laser power was always lower than the critical power for relativistic self-focusing when the pulse was chirped: $P/P_C<1$, where P_C(GW) $\simeq16.2(\omega_0/\omega_p)^2$ [15]. Therefore, the effective interaction length was never larger than a Rayleigh length $z_R=\pi w_0^2/\lambda_0=140$ μm. In addition, the pulse length $c\tau_c$ was always larger than z_R.

The time resolution dt of the method is limited by the spectral width $d\omega$ (at FWHM) of the Raman satellites. The spectral width can be due to the Fourier transform limit, in this case $dt\geqslant4\ln2/d\omega$; it can also be limited by the chirp, in this case $dt=d\omega/(2b)$. In the best case, the resolution is $dt=\sqrt{\tau_0\tau_c}$, which is 190 fs (460 fs) for a 1 ps (6 ps) chirped pulse. In this paper, the resolution is represented for each data point by error bars on the figures. It is generally lower than 1 ps and small enough so that $dt/\tau_c\leqslant0.3$.

The time of maximum scattering t_{RFS} (t_{RSS}) can be obtained from the spectra of forward scattered (30° side scattered) light. The results are presented in Fig. 2: both RFS (open squares) and 30° RSS (open diamonds) grow at the back of the pulse. It should be noted that the measurement could not resolve the difference in the growth of RFS and 30° RSS. In addition, the sign of the chirp does not seem to affect the growth of RFS and RSS: for a given pulse duration, the times of maximum scattering t_{RFS} and t_{RSS} are the same for a positive or a negative chirp. This is also confirmed by the fact that the Raman satellites have about the same amplitude for a positive or negative chirp (see Fig. 1). There is another interesting feature in Fig. 2: for long pulses ($\tau_c>4$ ps), the maximum scattering tends to occur around the middle of the pulse.

These results are in agreement with PIC simulations: Fig. 1(c) from Ref. [9] shows a simulation with parameters similar to ours: $\tau_{FWHM}=600$ fs, $a_0=0.3$, $n_e/n_c=1\%$. It clearly shows that in this regime, RFS takes place at the end of the pulse.

In order to explain the behavior of RFS for longer pulses ($\tau\geqslant1$ ps), we developed a simple temporal model. The chirped electric field is described as

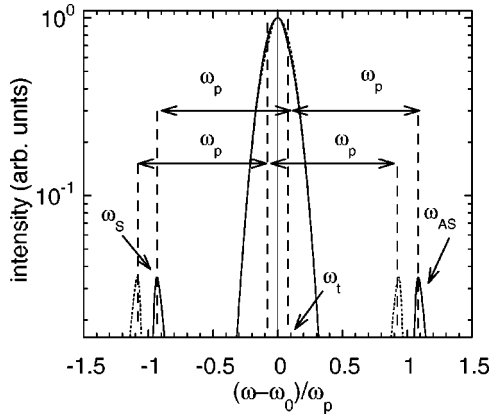

FIG. 3. Calculated RFS spectra for $\tau_c=4.2$ ps, $I=1.2\times10^{17}$ W/cm^2, $n_e=3\times10^{19}$ cm^{-3}. Solid (dotted) line: positive (negative) chirp.

$$E_{in}(t)=E_0\exp\left[-2\ln 2\left(\frac{t}{\tau_c}\right)^2+i\Phi\right], \tag{1}$$

where $\Phi=\omega_0 t+bt^2$. The plasma wave driven by RFS grows according to the purely temporal, nonrelativistic four wave growth rate [7] $\gamma_0=a_0(t)\omega_p^2/(\sqrt{8}\omega_0)$, where it is assumed that $a_0<1$, and $a_0(t)\propto\sqrt{I(t)\lambda^2}$. The plasma wave is also damped by the modulational instability (MI) in the supersonic regime [16] for which the growth rate is given by: $\alpha_0=(\omega_{pi}/\sqrt{6})(c/v_{th})\delta n(t)$. The evolution of the plasma wave can be found by solving the heuristic equation

$$\frac{\partial}{\partial t}\delta n=\gamma_0(t)\,\delta n-\alpha_0(t,\delta n)\,\delta n. \tag{2}$$

The first term on the right-hand side describes the growth of the plasma wave due to RFS. The instability is considered to be in its linear part and the wave amplitude is small: $\delta n\ll1$. It is also considered to be weak enough so that the envelope of the pulse is not modified ($\gamma_0/\omega_p\ll1$). The second term is a phenomenological term simulating the damping of the plasma wave by the MI with a time dependent damping rate $\alpha_0(t)$. The interaction length is chosen to be the Rayleigh length since there is no self-focusing: it is the region where the laser intensity is high and where the plasma waves can have significant amplitudes. From these assumptions, one can write the electric field after interaction: $E_{out}(t)=E_{in}(t)\exp(i\Psi)$, where Ψ is the phase experienced by the laser during propagation in the plasma; it is given by

$$\Psi=\pi\delta n(t)\frac{\omega_p}{\omega_0}\frac{z_R}{\lambda_p}\sin(\omega_p t). \tag{3}$$

The experimental parameters always verify $a_0<1$ and $\gamma_0/\omega_p\ll1$, and this simple model gives results in good agreement with the experimental data. Figure 3 shows a calculated RFS spectrum with the same experimental parameters as Fig. 1. For this calculation, the temperature was $T_e=200$ eV and the initial noise δn_0 was considered to be caused by the longitudinal ponderomotive force of a Gaussian pulse with truncated feet [17]: $\delta n_0=0.9\pi a_0^2/(\tau_c\omega_p)^{2.8}$.

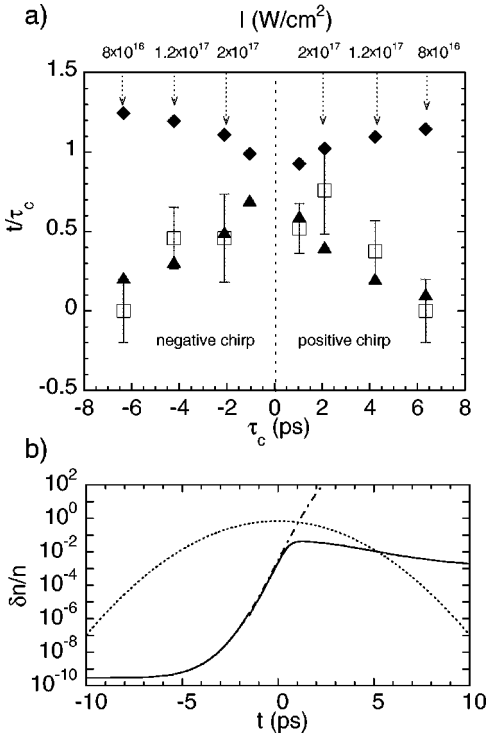

FIG. 4. (a) Time of maximum scattering for RFS for different pulse durations $n_e=3\times10^{19}$ cm^{-3}. Open squares, experimental data; closed triangles (diamonds), calculated points with (without) damping by the modulational instability. (b) Dotted line, profile of the laser pulse; solid (dash-dotted) line, growth of the plasma wave with (without) damping.

One can notice a remarkably good agreement between the experiment and the model in terms of the satellite positions and amplitude. For instance the relative amplitude of the Raman satellites is 2.5 to 4×10^{-2} in the experiment and 3.5×10^{-2} for the calculated spectrum. For the positive chirp, the position of the Stokes (anti-Stokes) is $\lambda_S=928$ nm ($\lambda_{AS}=708$ nm) for the experimental case, and $\lambda_S=926$ nm ($\lambda_{AS}=711$ nm) for the calculation. The free parameters T_e and δn_0 do not have an important effect on the result: changing T_e from 50 eV to 1 keV causes the Raman satellites to be shifted by less than 4 nm [which is 4×10^{-2} in units of $(\omega-\omega_0)/\omega_p$].

The same model was used to retrieve the time of maximum scattering for RFS as a function of pulse duration. A comparison between the model and the experiment is shown in Fig. 4(a): without MI (solid diamonds), the model predicts a growth of the plasma wave until the end of the pulse. In this case, the scattering takes place very late in the pulse, contrary to what is observed. When damping of the plasma wave by the MI is included, the agreement with the experimental result is very good. The growth of ion waves in a time of the order of a few ion plasma periods saturates the plasma wave amplitude at about 5%. This is shown in Fig. 4(b). Moreover, before being damped, the plasma wave grows as $\exp\Gamma(t)$, with

$$\Gamma(t)=\int_{-\infty}^{t}\gamma_0(t)dt\propto\sqrt{\tau_c}[1+\mathrm{erf}(t/\tau_c\sqrt{2\ln 2})]. \tag{4}$$

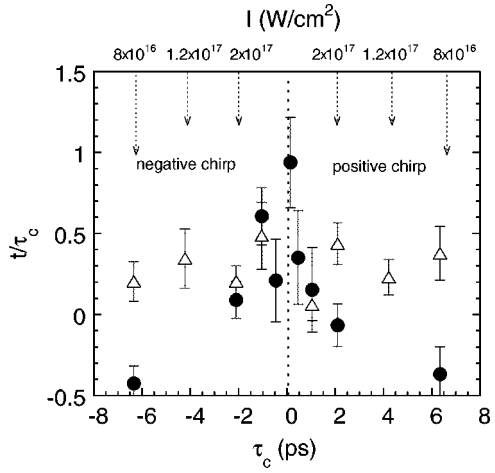

FIG. 5. Time of maximum scattering for RSS for different pulse durations and densities. Open triangles, experimental points for RSS at $n_e = 1.5 \times 10^{19}$ cm^{-3}; closed circles, experimental points for RSS at $n_e = 6 \times 10^{19}$ cm^{-3}.

This explains that for longer pulses, the plasma wave reaches high amplitudes earlier in the pulse reference frame. As a consequence, it is damped earlier. This is confirmed by Fig. 4(a).

In Fig. 5, the time of maximum scattering for 30° RSS is represented for two different densities. It shows that for long pulses, the maximum scattering occurs earlier in the pulse when the density is increased. This is due to the fact that for higher densities, RSS grows faster and the plasma wave reaches high amplitudes earlier in the pulse reference frame. Furthermore, at higher densities, ω_{pi} is larger; the ions can move faster and the MI is more efficient.

Measurements on RBS were also performed and showed that for $n_e = 1.2 \times 10^{19}$ cm^{-3}, RBS always occurred before the peak of the pulse. However, we found a difference in the time of maximum scattering for a positive and negative chirp. This could have been due to ionization blue shifting since RBS takes place at the beginning of the pulse. However, this point needs further investigations.

In conclusion, we have reported on measurements of Raman instabilities with subpicosecond time resolution in the referential frame of the laser pulse. We have found that Raman 30° side scattering and forward scattering occur at the back of the pulse. A simple model has been developed; it allows us to calculate RFS spectra with a good accuracy, and the results match the experiment very well. The model also shows that for long pulses, the plasma wave cannot have an amplitude larger than 5% because of the damping by the modulational instability. We have also shown that this damping occurs earlier at higher densities. These results are in agreement with previously published theoretical estimates and PIC simulations.

[1] J. F. Drake *et al.*, Phys. Fluids **17**, 778 (1974).
[2] T. Tajima and J. M. Dawson, Phys. Rev. Lett. **43**, 267 (1979).
[3] E. Esarey *et al.*, IEEE Trans. Plasma Sci. **24**, 252 (1996).
[4] N. E. Andreev *et al.*, Pis'ma Zh. Éksp. Teor. Fiz. **55**, 551 (1992) [JETP Lett. **55**, 571 (1992)]; P. Sprangle *et al.*, Phys. Rev. Lett. **69**, 2200 (1992).
[5] A. Modena *et al.*, Nature (London) **377**, 606 (1995); D. Umstadter *et al.*, Science **273**, 472 (1996).
[6] M. Tabak *et al.*, Phys. Plasmas **1**, 1626 (1994).
[7] W. L. Kruer, *The Physics of Laser Plasma Interaction* (Addison-Wesley, Reading, MA, 1988), Chap. 7, p. 78-79.
[8] K. C. Tzeng, W. B. Mori, and T. Katsouleas, Phys. Plasmas **6**, 2105 (1999).
[9] K. C. Tzeng, W. B. Mori, and C. Decker, Phys. Rev. Lett. **76**, 3332 (1996).
[10] P. Bertrand *et al.*, Phys. Plasmas **2**, 3115 (1995); C. I. Moore *et al.*, Phys. Rev. Lett. **79**, 3909 (1997).
[11] A. Ting *et al.*, Phys. Rev. Lett. **77**, 5377 (1996); S. P. Leblanc *et al.*, *ibid.* **77**, 5381 (1996).
[12] P. Chessa *et al.*, Phys. Rev. Lett. **82**, 552 (1999).
[13] V. Malka *et al.*, Rev. Sci. Instrum. **71**, 6 (2000).
[14] N. Bloembergen, Opt. Commun. **8**, 285 (1973); S. C. Rae and K. Burnett, Phys. Rev. A **46**, 1084 (1992); W. M. Wood, G. Focht, and M. C. Downer, Opt. Lett. **13**, 984 (1988).
[15] A. G. Litvak, Zh. Éksp. Teor. Fiz. **57**, 629 (1969) [Sov. Phys. JETP **30**, 344 (1969)]; P. Sprangle, C. M. Tang, and E. Esarey, IEEE Trans. Plasma Sci. **15**, 145 (1987).
[16] F. Amiranoff *et al.*, Phys. Rev. Lett. **68**, 3710 (1992); V. E. Zakharov, Zh. Éksp. Teor. Fiz. **62**, 1745 (1972) [Sov. Phys. JETP **35**, 908 (1972)]; P. Mora *et al.*, Phys. Rev. Lett. **61**, 1611 (1988).
[17] C. D. Decker, Ph.D. dissertation, University of California, Los Angeles, 1994, p. 115.